Design, Simulation, Validation and Comparison of New High Step-up Soft Switched Converter for Fuel Cell Energy System

N.KARAMI[1], H.TORKAMAN[2], AND M.M.NEZAMABADI[3]

[1,2] *1Faculty of Electrical Engineering, Shahid Beheshti University, A.C., Tehran, Iran. 1658953571*
[3] *Department of Electrical Engineering, Islamic Azad University, West Tehran Branch, Tehran, Iran.*
[*] *Corresponding author:H_torkaman@sbu.ac.ir*

Manuscript received May 12, 2017; revised July 4: accepted July 14, 2017. Paper no. JEMT1705-1013

Fuel cell energy systems can deliver green energy efficiently without CO2 emissions, which are nominated as a substitution choice for the conventional power sources. This paper proposes a new high step-up DC-DC converter which is applicable in distributed energy resources, especially for fuel cell power conditioning systems. The converter contains a bidirectional boost cell with a coupled inductor, two transformers whose secondary sides are connected in series to increase the voltage gain and also a voltage doubler. Leakage inductance of the coupled inductor limits the currents of output diodes and results in Zero Current Switching (ZCS) of the diodes. The converter schematic is presented at first and then its analysis results in different modes of operation are given. After that the theoretical formulation of voltage gain are achieved and proved. Finally, simulations results for a 400 W/ 380 V load are presented to validate the claimed characteristics of the proposed converter.

keywords: *Fuel Cell, High Step-up Converter, Zero Current Switching, Zero Voltage Switching, Simulation.*

http://dx.doi.org/10.22109/JEMT.2017.49433

1. INTRODUCTION

New energy resources, including Photovoltaic (PV), Wind turbines (WT), Fuel Cells (FCs), etc. have attracted the researchers over the past few years [1, 2]. In this regard, FCs are prominent energy resources which are accentuated by specific characteristics that make them distinguished among their counterparts [3–5]. The sensitivity of operation against the output current ripple and slow transient response are the important characteristics of FCs [6,7]. Since the electrical energy produced by FCs is Direct Current (DC), an inverter module is required for its connection to the power network [8,9]. Many high gain dc-dc converters are proposed in recent years to be used as power conditioning system for FCs [10,11]. Due to the mentioned characteristics of FCs, the high step-up DC-DC converters used in power conditioning systems for FCs should have some special features [12] which are listed as follows:

• High voltage gain, to prepare the DC-link for grid connected inverters;

• Low ripple input current, to achieve high efficiency and long life-time of FCs;

• Soft switching operation to decrease the switching losses of power semiconductors.

Utilization of the various DC-DC converter topologies [13,14] in renewable energy (RE) systems is increasing in order to generate a reliable and controllable dc output to match a variable or fixed load demand [15–17]. In [18] a high step-up DC-DC converter is proposed. Despite having a high voltage gain in this converter, it has some drawbacks like the voltage stress of diode D-3 and high ripple input current which affects FCs efficiency and life time. In [19], a new converter is proposed whose switches do not have voltage stress but still the input current has high ripple that degrades the operation of the converter. In [20] a converter is proposed which has high voltage gain with ripple free input current. This converter contains four switches which results in two more gate drivers and more losses. In [21], a two-directional converter for FC application is presented. In which, an ultra-capacitor is utilized for energy storing, which leads to the FC better control response time. A hybrid FC power system is presented in [22,23] in which two-directional and unidirectional converters are connected to the battery and FC to achieve better efficiency.

A typical FC energy system is demonstrated in Figure 1. Due to a low voltage produced from FC, a high step-up DC-DC converter is needed to enhance the generated voltage in specific applications. Generally, a classic boost dc-dc converter could be implemented to provide a high step-up gain along-

side the proper duty ratio [24]. Nevertheless, the voltage gain and the efficiency are restricted due to the losses of diodes and power switches [25]. Consequently, a step-up dc-dc converter with minimum switching losses and suitable duty ratio is necessary for FC power system to provide high voltage gain and efficiency [26,27]. Therefore, in this paper a new high step-up DC-DC converter is proposed for FC power conditioning systems which decreases the current ripple and increases the FC efficiency o. Due to voltage gain of the converter the use of FCs in grid connected applications becomes possible. In this paper the operation modes of the proposed converter are described in Section 2 and the required equations to achieve a ripple free input current is discussed. Voltage gain of the converter is calculated and shown in section 3. Section 4 compares the converter with current fed full bridge converter. Implementation results are shown in section 5 to confirm soft switching operation and the applicability of the converter. Finally, the conclusions of this study are presented in section 6.

2. NEW CONVERTER AND OPERATION MODES

The power system block diagram including FCs as one of its resources is illustrated in Figure 1.

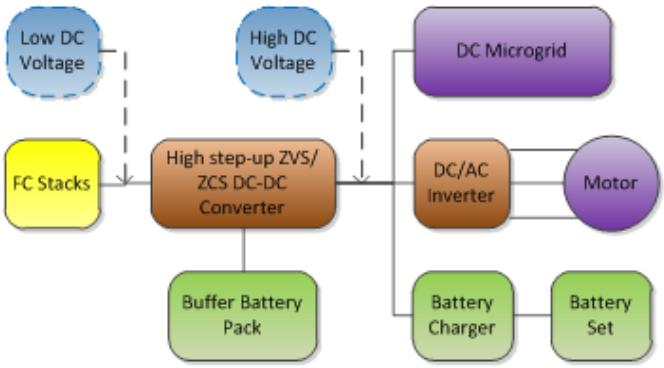

Fig. 1. Configuration of a FC power system

The limitations for FC are considered as follows: (a) don't accepct the minus current, (b) the current ripple higher than 400Hz will have minimum side effect on FC, (c) the current ripple lower than 4

As shown in Figure 1 a high step up DC-DC converter is required for connecting FC to the power network. The proposed converter (Figure 2) contains two switches S¬1 and S2 which operate based on PWM switching strategy for obtaining high voltage gain and ripple free input current.

The coupled inductor is used to cancel the input current ripple. Two transformers are located in the circuit with their secondary sides connected in series to increase the voltage gain of the converter and to isolate the low voltage side of the converter from the high voltage side. The voltage doubler at the output side of the converter is for increasing the secondary side voltage of the transformers and also regulating the output voltage. The coupled inductor and boosting transformers are modeled as ideal transformers with magnetizing inductance at the primary side and leakage inductance at the secondary side of the transformers. The turn's ratio of the coupled inductor is $n = N_s/N_p$ and the turns ratios of transformers are $n_1 = N_{s1}/N_{p1}$ and $n_2 = N_{s2}/N_{p2}$.To analyze the proposed converter it is assumed that:

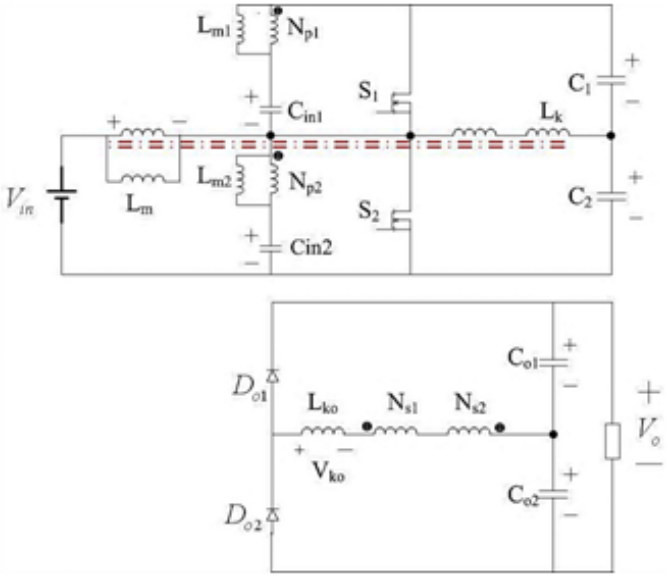

Fig. 2. Proposed converter

- Switches and diodes are ideal
- Capacitors and inductors have no parasitic effects.
- Voltage ripple of capacitors is very small.

At the time t_0 the converter has the following initial conditions;

$$i_m = i_m^{\min},\ i_k = i_k^{\max},\ i_{ko} = i_{ko}^{\max},\ i_{m1} = -i_{m2} = -I_m \quad \textbf{(1)}$$

Figure 3 and Figure 4 illustrate the operation modes and key waveforms of the proposed converter, respectively. Mode 1: **[?, ?]** This mode starts when S2 is turned on. According to Figure 4, the body diode of S_2 has been turned on before the gate pulse of S_2 is applied, so S_2 is turned on in zero voltage switching condition. In this mode D_{O1} is on and S_1 and D_{O2} are off, simultaneously. In this regard, equations related to this mode are as follows:

$$i_m = i_m^{\min} + \frac{V_{in}}{L_m}(t - t_0) \quad \textbf{(2)}$$

$$i_{m1} = -I_m + \frac{V_{in}}{L_m}(t - t_0) \quad \textbf{(3)}$$

$$i_{m1} = -I_m + \frac{V_{in}}{L_m}(t - t_0) i_{m2} = I_m - \frac{V_{in}}{L_m}(t - t_0) \quad \textbf{(4)}$$

$$i_k = i_k^{\max} + \frac{(n-1)V_{in}}{L_k}(t - t_0) \quad \textbf{(5)}$$

$$i_k = i_k^{\max} + \frac{(n-1)V_{in}}{L_k}(t - t_0) \quad \textbf{(6)}$$

This mode is finished when iko becomes zero. Hence D_{O1} turned off and D_{O2} turned on. Due to the leakage inductances of the transformers, the current of D_{o1} decreases to zero, and the diode is turned off in zero current switching condition.

Mode 2: $[t_1, t_2]$ In this mode D_O2 and S_2 are on and other semiconductor devices are off. The current of the magnetizing inductance of coupled inductor increases and the current of leakage inductance of coupled inductor decreases.

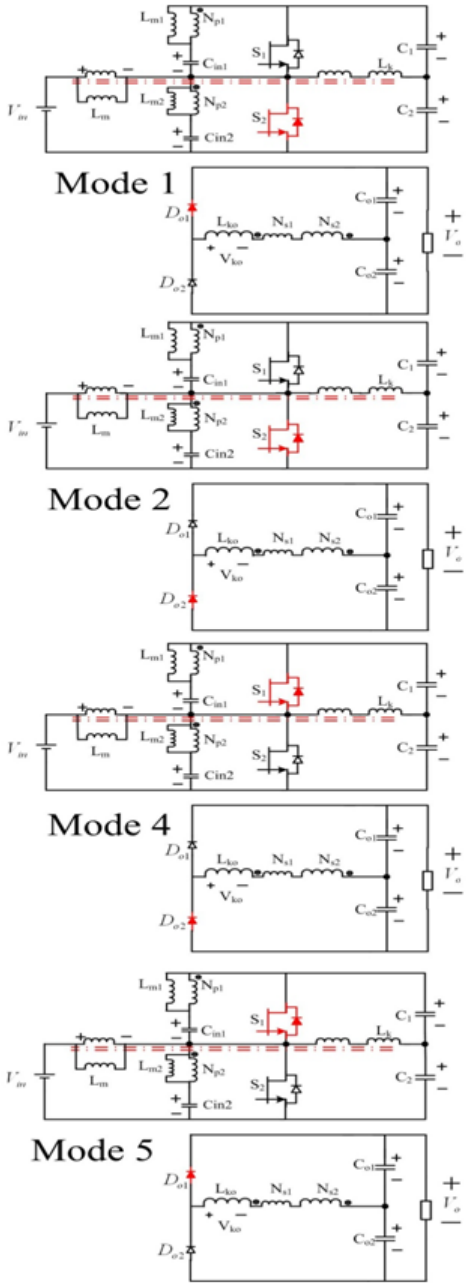

Fig. 3. Operation modes of the proposed converter.

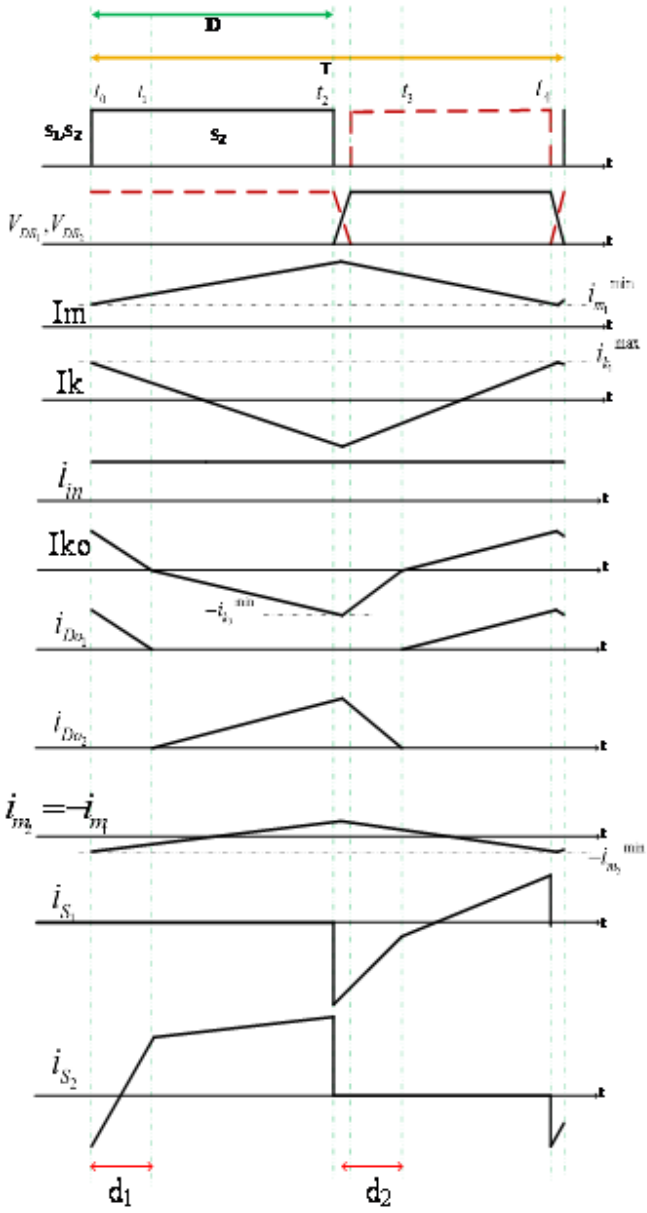

Fig. 4. Main waveforms.

So the mathematical relations of this mode are similar to mode 1 except for:

$$i_{ko} = \frac{V_{o1} - (n_1 + n_2)V_{in}}{L_{ko}}(t - t_1) \quad \textbf{(7)}$$

This mode finishes when the switch S_2 is turned off.

Mode 3: At the beginning of this mode S_2 is turned off and both switches remain off during this interval. The current of S_2 discharges the Drain-Source capacitor of S_1, charges the Drain-Source capacitor of S_2 and then flows through the body diode of switch S_1. This mode occurs very fast. When the current flows through the body diode of S_1, the voltage across this switch becomes zero and this switch is ready to be turned on in ZVS condition.

Mode 4: $[t_2, t_3]$ This mode occurs when the S1 is turned on in ZVS condition. In this mode, D_{O2} is on and S_2 and D_{O1} are off, simultaneously. Also, the current of Dz_{o2} decreases. The equations related to this mode are as follows:

$$i_m = i_m(t_2) - \frac{D}{1-D}\frac{V_{in}}{L_m}(t - t_2) \quad \textbf{(8)}$$

$$i_{m1} = i_{m1}(t_2) - \frac{D}{1-D}\frac{V_{in}}{L_m}(t - t_2) \quad \textbf{(9)}$$

$$i_{m2} = i_{m2}(t_2) + \frac{D}{1-D}\frac{V_{in}}{L_m}(t - t_2) \quad \textbf{(10)}$$

$$i_k = i_k(t_2) - \frac{(n-1)DV_{in}}{(1-D)L_k}(t - t_2) \quad \textbf{(11)}$$

$$i_{ko} = i_{ko}(t_2) + \frac{\frac{D}{1-D}(n_1 + n_2)V_{in} + V_{o1}}{L_{ko}}(t - t_2) \quad \textbf{(12)}$$

Mode 5: $[t_3, t_4]$ this mode starts when D_{o2} turned off in ZCS condition. In this modeD_{O1} and S_1 are on and other semiconductor devices are off. So the mathematical relations of this mode are similar to mode 4 except for:

$$i_{ko} = i_{ko}(t_2) + \frac{\frac{D}{1-D}(n_1+n_2)V_{in} + V_{o1}}{L_{ko}}(t-t_2) \quad (13)$$

Mode 6: At the beginning of this mode S_1 is turned off and both switches remain off, during this interval. The current of S_1 discharges the Drain-Source capacitor of S_2, charges the Drain-Source capacitor of S_1 and then flows through the body diode of S_2. This mode occurs very fast.

When the current flows through the body diode of switch S_2, the voltage across this switch becomes zero and this switch is ready to be turned on in ZVS condition.

A. Input current ripple cancelation condition

FCs are sensitive to the ripple of their output current. In this subsection the ripple cancelation condition of the proposed converter is derived. According to (2) and (5) the input current is derived as follows:

$$i_{in} = i_m^{\min} + n\, i_k^{\max} + \left(\frac{V_{in}}{L_m} + n\,\frac{(n-1)V_{in}}{L_k}\right)(t-t_0) \quad (14)$$

Hence, to achieve the ripple free input current, it is necessary that the current slope in equation (14) becomes zero that implies:

$$L_k = L_m \times\ n\ (1-n) \quad (15)$$

Equation (15) is the required condition to achieve ripple free input current. Due to the complexity to achieve (15) in the practical inductor design, it is possible to use a series inductance to compensate the required condition mentioned in equation(15).

3. VOLTAGE GAIN EVALUATION

High amplitude of voltage gain is a key advantage of the new converter, which is assessed and presented in this part. The output voltage of the converter is the summation of C_{o1} and C_{o2} voltages, and is calculated by the voltage balance of the inductors. The output voltage of the proposed converter can be obtained by:

$$V_o = V_{o1} + V_{o2} \quad (16)$$

According to the maximum value for the output diodes current, V_{o1} and V_{o2} are calculated as follows:

$$V_{o1} = \frac{(n_1+n_2)V_{in}}{1-D}\left(1 - D - \frac{d_2}{(D-d_1+d_2)}\right) \quad (17)$$

$$V_{o2} = \frac{(n_1+n_2)V_{in}}{1-D}\left(D - \frac{d_1}{(1-D-d_2+d_1)}\right) \quad (18)$$

So the output voltage of the converter can be derived from (19).

$$V_o = \frac{(n_1+n_2)V_{in}}{1-D}\left(1 - \frac{d_1}{(1-D-d_2+d_1)} - \frac{d_2}{(D-d_1+d_2)}\right) \quad (19)$$

To determine the voltage gain of the converter d_1 and d_2 are obtained using the fact that the output current is equal to the average current that flows through D_{o1} and D_{o2}. Therefore the voltage gain of the proposed converter can be calculated from (20).

$$\frac{V_o}{V_{in}} = \frac{(n_1+n_2)}{1-D} \times \times \left(1 - \frac{kD}{(1-k)(1-D)+kD} - \frac{k(1-D)}{(1-k)D+k(1-D)}\right) \quad (20)$$

in which k is represented as the following:

$$m = \frac{L_{ko}I_o}{(n_1+n_2)TV_{in}}$$
$$d_1 = \frac{1}{2}\left(1 - \sqrt{1-\frac{4m}{D}}\right)D = kD \quad (21)$$
$$d_2 = \frac{1}{2}\left(1 - \sqrt{1-\frac{4m}{D}}\right)(1-D) = k(1-D)$$

Figure 5 illustrates the voltage gain versus duty cycle D with respect to variation of n_2.

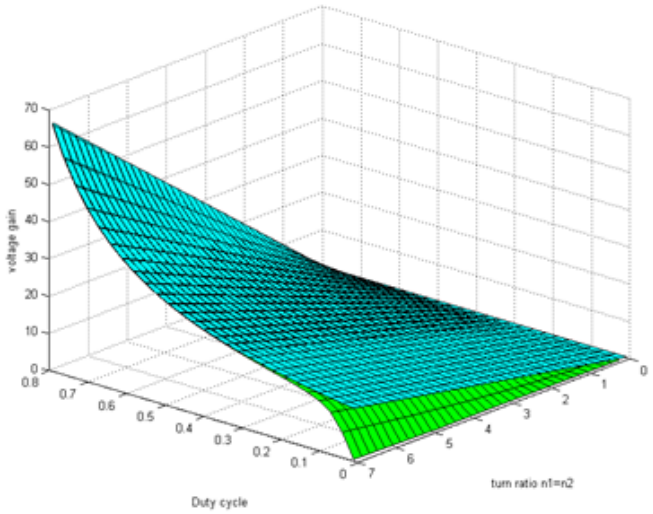

Fig. 5. voltage gain versus duty cycle and turns ratio n_2.

4. COMPARATIVE STUDY

Current-fed full bridge DC-DC converter is a well-known converter for power conditioning systems for FCs [28, 29]. In this section the proposed converter is compared with CFFB- Active Clamp converter and the converter proposed in [10].

The comparison results are summarized in Table 1. According to Table 1 the number of switches and diodes of the proposed converter is less than the power semiconductors of CFFB converter. Also the number of switches is less in comparison with the converter presented in [10] that implies a lower number of drive circuits in the proposed converter.

According to Table 1 the number of switches and diodes of the converter (2,2) is less than the CFFB converter (5,4). Therefore, the total stress is less in proposed converter (2VstressS +2 VstressD) in comparison with CFFB (5VstressS,4 VstressD) and Ref. [10].

Duty cycle of the proposed converter can vary in a wider range with respect to CFFB converter while the voltage gain is not larger than 2n, for CFFB converter. So for achieving high voltage gain specification, it is required to increase the turn ratios of the transformer. Figure 6 illustrates the proposed converter current in comparison with the relative current in [10]. According to Figure 6 although the output power flows through two

Table 1. comparison of the proposed converter versus CFFB with Active Clamping

Converter/Feature	CFFB with Active Clamping	Ref [10]	Proposed converter
Duty cycle	$0.5 < D < 1$	$0 < D < 1$	$0 < D < 1$
# Switches	5	4	2
# Diodes	4	2	2
# magnetic elements	2	2	3
Voltage stress of switches	$\frac{V_{in}}{3/2-D}$	$\frac{V_{in}}{1-D}$	$\frac{V_{in}}{1-D}$
Voltage stress of diodes	V_o	V_o	V_o
Ideal voltage gain	$\frac{n}{3/2-D}$	$\frac{2n}{1-D}$	$\frac{2n}{1-D}$

switches, the current remains with the same maximum value. Also maximum value of S1current increases (Figure 7) and as a result the ZVS of this switch increases. Because of the similarity of the diodes' currents, the proposed converter and the converter in [10] have the same diode losses.

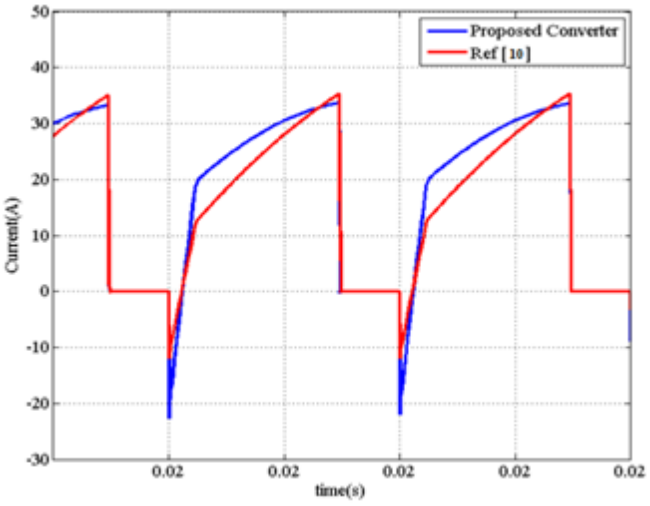

Fig. 6. Comparing current of switch S2 with the relative switch

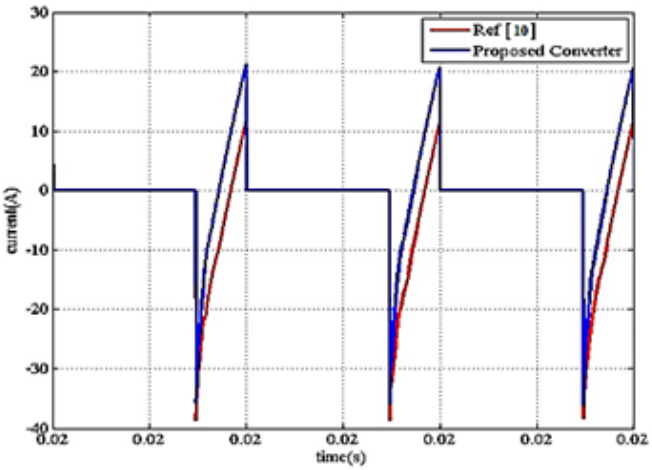

Fig. 7. Comparing current of switch S1 with the relative switch.

5. SIMULATION RESULTS FOR THE PROPOSED CONVERTER

In this section the simulation results are presented to validate characteristics of the proposed converter. The new converter is utilized to supply a 450 W resistive load. Input voltage was selected as 30V and maximum duty cycle ($D = 0.71$) occurred at full load operation in which maximum Drain-source voltage of switches is less than 98V.

IRFP4332PBF MOSFET is selected for this application, whose Coss is 800pF. The switching frequency is 100 kHz, so fast reverse recovery Schottky diode, MUR860, is selected as output diodes Do1 and Do2. Film-low ESR 33uF capacitors are utilized in the topology. Magnetizing inductances are $L_m = L_{m1} = L_{m2} = 100\mu H$ and $L_k = 70\mu H$ and the turns ratio of transformers is $n2 = n1 = 3$. The simulation is performed in OrCAD Capture 16.6 environment.

Fig. 8 illustrates the converter output voltage with respect to the input voltage, in time domain. According to this figure the output voltage is regulated at 380 V in full load condition. Fig. 9 illustrates the input current of the converter. This figure demonstrates the current ripple cancelation feature of the converter. Fig. 10 and Fig. 11 demonstrate the ZVS operation of S_1 and S_2, respectively. Finally, Fig. 12 and Fig. 13 are presented to validate the ZCS operation of the converter output diodes.

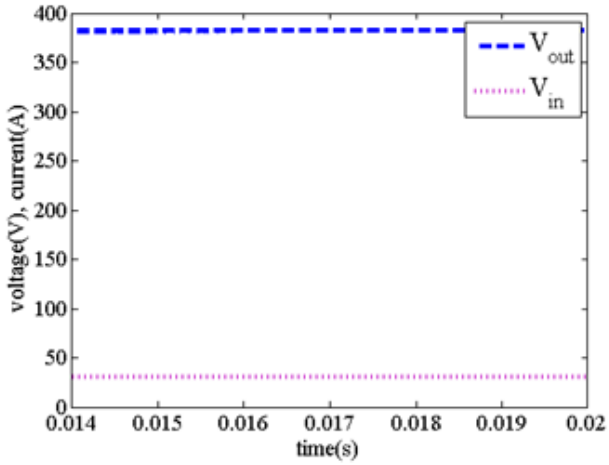

Fig. 8. Output and input voltage

Another important test of the proposed converter is transient response of the converter in open loop condition. This test is used to show the stability of converter when a transient response occurs in the converter. In this test which is shown in Fig. 14, the output load is changed from 200W to 400W and the transient response of the input current and output voltage (Vout is divided by 20 for measurement) are illustrated in this figure.

The main components of the power losses include switches and diode losses. These parameters are evaluated by simulation in switches' current of both converter in the same condition. Because of the similarity of the diodes' currents, the proposed converter and the converters in [10] have the same diode losses (Fig.12, 13). According to Fig.6, although the output power flows through two switches, the current remains with the same maximum value. Also, maximum value of the S1's current increases (Fig.7) and as a result the ZVS of this switch increases. Furthermore, S1 in the new converter has more turn off losses, but other converter has two more switches, therefore its total

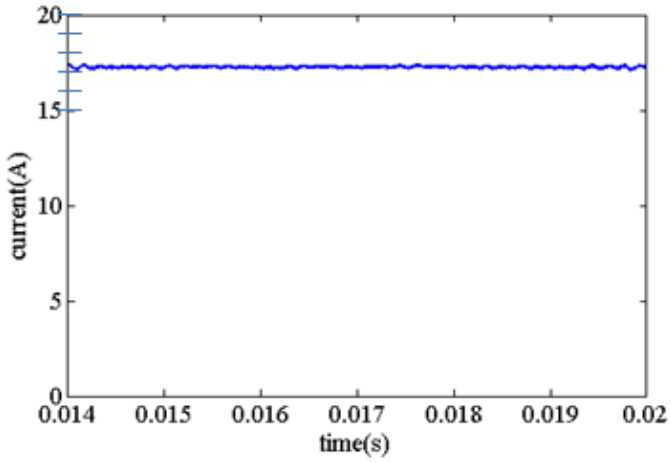

Fig. 9. input current

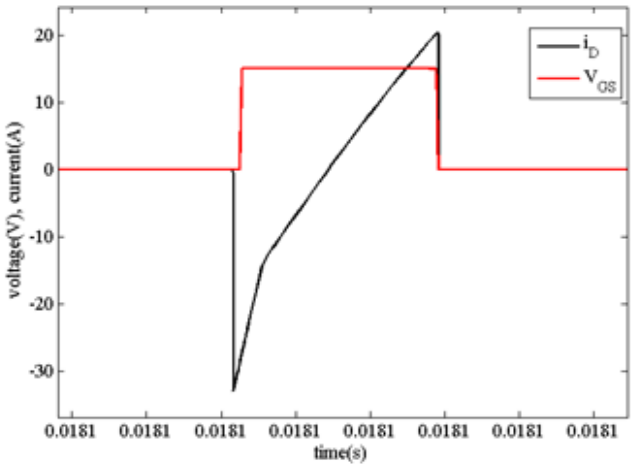

Fig. 10. ZVS validation of switch S1

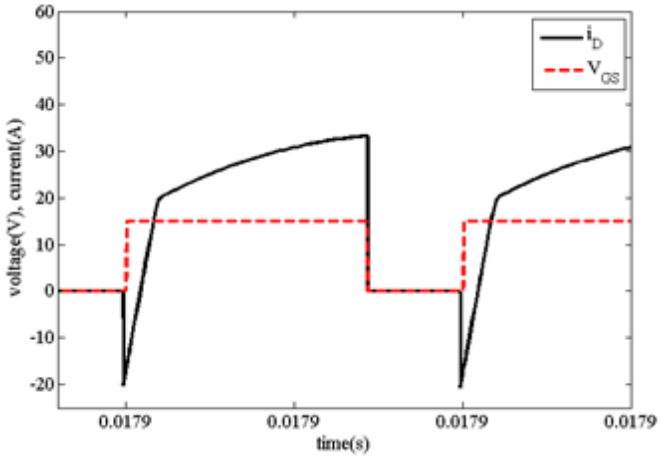

Fig. 11. ZVS validation of switch S2

power losses is more than proposed converter.

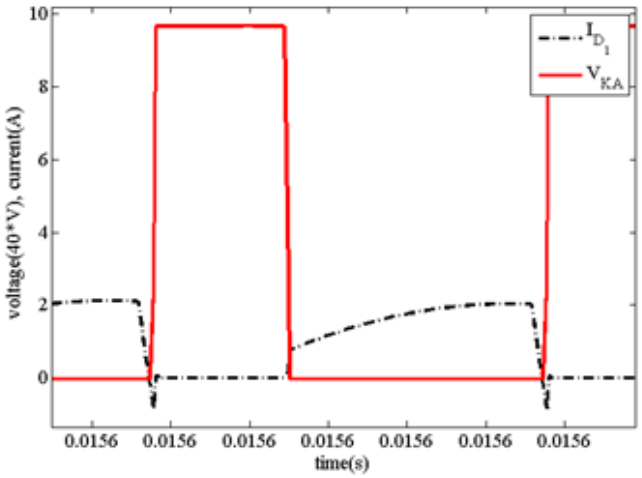

Fig. 12. ZCS of Diode Do1

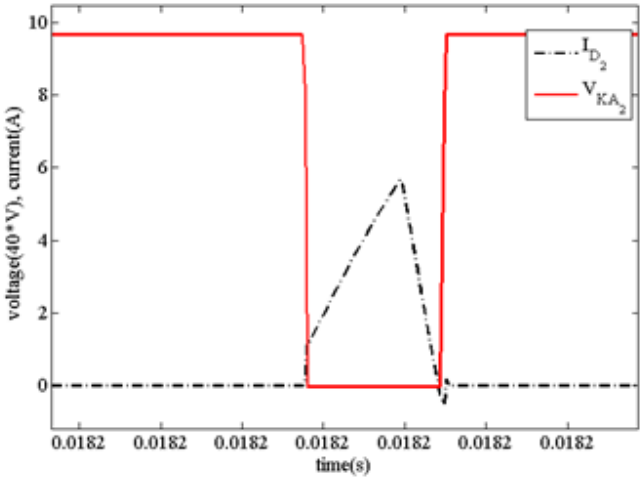

Fig. 13. ZCS of Diode Do2

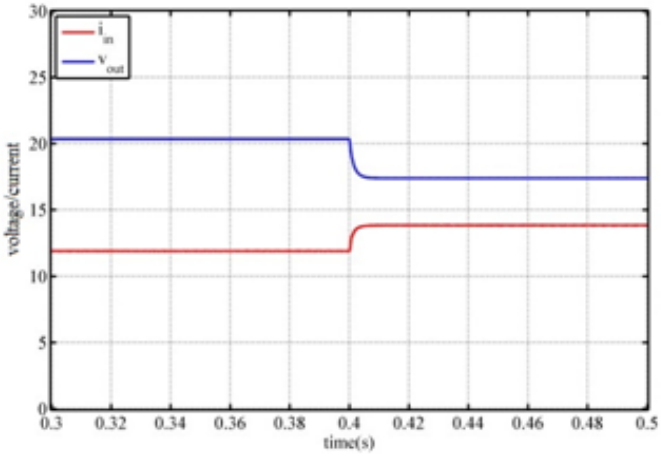

Fig. 14. Transient response of the converter

6. CONCLUSION

A new high gain DC-DC converter is presented and analyzed in details, in this paper. The main features of the proposed

converter are listed as follows: (a) ripple free input current, (b) high voltage gain, (c) soft switching operation, (d) fewer number of semiconductor, (e) wide range of duty cycle and (f) isolation of FC and the high voltage DC-link. Mathematical equations governing the operation, such as the equations of the converter different modes and the voltage gain of the converter are presented. In order to validate the characteristics of the proposed converter, the converter operation is simulated in the OrCAD Capture environment and the results were given. The converter is equipped with two transformers to increase the voltage gain and isolate low side and high side of the converter. Coupled inductor was used to eliminate the input current ripple and the transformer leakage inductance is used to provide the converter ZCS operation.

REFERENCES

1. X. Zhang, H. Ren, S. Pyo, J.-I. Lee, J. Kim, and J. Chae, "A high-efficiency dc–dc boost converter for a miniaturized microbial fuel cell," *IEEE Transactions on Power Electronics*, vol. 30, no. 4, pp. 2041–2049, 2015.
2. Y. Cho and J.-S. Lai, "High-efficiency multiphase dc–dc converter for fuel-cell-powered truck auxiliary power unit," *IEEE Transactions on Vehicular Technology*, vol. 62, no. 6, pp. 2421–2429, 2013.
3. Y. Park, B. Jung, and S. Choi, "Nonisolated zvzcs resonant pwm dc–dc converter for high step-up and high-power applications," *IEEE Transactions on Power Electronics*, vol. 27, no. 8, pp. 3568–3575, 2012.
4. S. Lee, P. Kim, and S. Choi, "High step-up soft-switched converters using voltage multiplier cells," *IEEE Transactions on Power Electronics*, vol. 28, no. 7, pp. 3379–3387, 2013.
5. G. Wu, X. Ruan, and Z. Ye, "Nonisolated high step-up dc–dc converters adopting switched-capacitor cell," *IEEE Transactions on Industrial Electronics*, vol. 62, no. 1, pp. 383–393, 2015.
6. Q. Wu, Q. Wang, J. Xu, H. Li, and L. Xiao, "A high efficiency step-up current-fed push-pull quasi-resonant converter with fewer components for fuel cell application," *IEEE Transactions on Industrial Electronics*, 2016.
7. R.-J. Wai and C.-Y. Lin, "High-efficiency, high-step-up dc–dc convertor for fuel-cell generation system," *IEE Proceedings-Electric Power Applications*, vol. 152, no. 5, pp. 1371–1378, 2005.
8. N. Molavi, E. Adib, and H. Farzanehfard, "Soft-switched non-isolated high step-up dc–dc converter with reduced voltage stress," *IET Power Electronics*, vol. 9, no. 8, pp. 1711–1718, 2016.
9. M. R. A. Siddique, M. J. Ferdous, and I. Islam, "Switched capacitor based soft-switching dc-dc boost converter for high voltage gain," in *Electrical and Computer Engineering (ICECE), 2014 International Conference on*, pp. 820–823, IEEE, 2014.
10. H.-L. Do, "Improved zvs dc-dc converter with a high voltage gain and a ripple-free input current," *IEEE Transactions on Circuits and Systems I: Regular Papers*, vol. 59, no. 4, pp. 846–853, 2012.
11. P. Thounthong and B. Davat, "Study of a multiphase interleaved step-up converter for fuel cell high power applications," *Energy Conversion and Management*, vol. 51, no. 4, pp. 826–832, 2010.
12. M. Delshad and H. Farzanehfard, "A new soft switched push pull current fed converter for fuel cell applications," *Energy Conversion and Management*, vol. 52, no. 2, pp. 917–923, 2011.
13. A. Khoudiri, K. Guesmi, and D. Mahi, "Spectral decomposition based approach for dc–dc converters modeling," *International Journal of Electrical Power & Energy Systems*, vol. 61, pp. 288–297, 2014.
14. L. Kumar and S. Jain, "A multiple source dc/dc converter topology," *International Journal of Electrical Power & Energy Systems*, vol. 51, pp. 278–291, 2013.
15. N. Jayaram, P. Agarwal, and S. Das, "Mathematical model of five-level ac/dc converter in abc reference frame," *International Journal of Electrical Power & Energy Systems*, vol. 62, pp. 469–475, 2014.
16. M. Nachidi, A. El Hajjaji, and J. Bosche, "An enhanced control approach for dc–dc converters," *International Journal of Electrical Power & Energy Systems*, vol. 45, no. 1, pp. 404–412, 2013.
17. R. Maurya, S. Srivastava, and P. Agarwal, "Symmetrical and asymmetrical controlled three-phase high frequency isolated dc–dc converter," *International Journal of Electrical Power & Energy Systems*, vol. 52, pp. 132–142, 2013.
18. B. Lin and J. Dong, "New zero-voltage switching dc–dc converter for renewable energy conversion systems," *IET Power Electronics*, vol. 5, no. 4, pp. 393–400, 2012.
19. Y.-P. Hsieh, J.-F. Chen, L.-S. Yang, C.-Y. Wu, and W.-S. Liu, "High-conversion-ratio bidirectional dc–dc converter with coupled inductor," *IEEE Transactions on Industrial Electronics*, vol. 61, no. 1, pp. 210–222, 2014.
20. J.-M. Kwon, E.-H. Kim, B.-H. Kwon, and K.-H. Nam, "High-efficiency fuel cell power conditioning system with input current ripple reduction," *IEEE Transactions on Industrial Electronics*, vol. 56, no. 3, pp. 826–834, 2009.
21. A. S. Samosir and A. H. M. Yatim, "Implementation of dynamic evolution control of bidirectional dc–dc converter for interfacing ultracapacitor energy storage to fuel-cell system," *IEEE Transactions on Industrial Electronics*, vol. 57, no. 10, pp. 3468–3473, 2010.
22. K. Jin, X. Ruan, M. Yang, and M. Xu, "A hybrid fuel cell power system," *IEEE Transactions on Industrial Electronics*, vol. 56, no. 4, pp. 1212–1222, 2009.
23. W.-S. Liu, J.-F. Chen, T.-J. Liang, and R.-L. Lin, "Multicascoded sources for a high-efficiency fuel-cell hybrid power system in high-voltage application," *IEEE Transactions on Power Electronics*, vol. 26, no. 3, pp. 931–942, 2011.
24. S.-J. Cheng, Y.-K. Lo, H.-J. Chiu, and S.-W. Kuo, "High-efficiency digital-controlled interleaved power converter for high-power pem fuel-cell applications," *IEEE transactions on industrial electronics*, vol. 60, no. 2, pp. 773–780, 2013.

25. U. R. Prasanna, A. K. Rathore, and S. K. Mazumder, "Novel zero-current-switching current-fed half-bridge isolated dc/dc converter for fuel-cell-based applications," *IEEE Transactions on Industry Applications*, vol. 49, no. 4, pp. 1658–1668, 2013.

26. C. de Beer, P. Barendse, and A. Khan, "Development of an ht pem fuel cell emulator using a multiphase interleaved dc–dc converter topology," *IEEE Transactions on Power Electronics*, vol. 28, no. 3, pp. 1120–1131, 2013.

27. N. A. Ahmed, M. Miyatake, and A. Al-Othman, "Power fluctuations suppression of stand-alone hybrid generation combining solar photovoltaic/wind turbine and fuel cell systems," *Energy Conversion and Management*, vol. 49, no. 10, pp. 2711–2719, 2008.

28. P. Xuewei and A. K. Rathore, "Novel bidirectional snubberless naturally commutated soft-switching current-fed full-bridge isolated dc/dc converter for fuel cell vehicles," *IEEE Transactions on Industrial Electronics*, vol. 61, no. 5, pp. 2307–2315, 2014.

29. P. Xuewei and A. K. Rathore, "Novel interleaved bidirectional snubberless soft-switching current-fed full-bridge voltage doubler for fuel-cell vehicles," *IEEE Transactions on Power Electronics*, vol. 28, no. 12, pp. 5535–5546, 2013.